Hindawi
International Journal of Photoenergy
Volume 2020, Article ID 8827917, 10 pages
https://doi.org/10.1155/2020/8827917

Research Article

Performance and Stability Comparison of Low-Cost Mixed Halide Perovskite Solar Cells: $CH_3NH_3PbI_{3-x}Cl_x$ and $CH_3NH_3PbI_{3-x}SCN_x$

Nji Raden Poespawati, Junivan Sulistianto, Tomy Abuzairi, and Retno Wigajatri Purnamaningsih

Department of Electrical Engineering, Faculty of Engineering, Universitas Indonesia, Depok 16424, Indonesia

Correspondence should be addressed to Nji Raden Poespawati; pupu@eng.ui.ac.id

Received 24 July 2020; Revised 5 September 2020; Accepted 23 September 2020; Published 13 October 2020

Academic Editor: Vishal Mehta

Perovskite solar cell is categorized as a third-generation solar cell which is used for its high-performance and low-cost production. However, device stability is a major problem in the development of perovskite solar cells. Mixed halide perovskite is one of the subjects that have been proposed to improve perovskite solar cell stability. Research about solar cells using mixed halide perovskite is widely reported. However, complex configurations and fabrication using sophisticated equipment were usually used in those reported studies. In this work, the fabrication of solar cells using mixed halide perovskite $CH_3NH_3PbI_{3-x}Cl_x$ and $CH_3NH_3PbI_{3-x}SCN_x$ was conducted using a simple and low-cost structure. Solution-processed deposition fabrication method using spin coating was used to fabricate the devices. Optimization of the spin coating rate for each layer in the perovskite solar cells was performed to ensure that the devices exhibited decent performance. Stability measurement and analysis of the perovskite solar cells were conducted. Summarily, solar cells with mixed halide perovskite $CH_3NH_3PbI_{3-x}Cl_x$ exhibit the highest performance with an efficiency of 2.92%. On the other hand, solar cell with mixed halide perovskite $CH_3NH_3PbI_{3-x}SCN_x$ has the best stability which only drops its efficiency by 39% from its initial value after 13 days.

1. Introduction

Perovskite material with a general formula of ABX_3 (where A is organic cation, B is divalent metal, and X is halide) has piqued the interest of many researchers, notably in the solar cell field. The first introduction to perovskite solar cell came from Akihiro et al. in 2009 with a device efficiency of 3.8% [1]. Originally, perovskite was used as sensitizer in dye-sensitized solar cell where perovskite with the formula $CH_3NH_3PbX_3$ (X was I or Br) was used. As a result, perovskite with $CH_3NH_3PbI_3$ yielded better efficiency. After ten years of its first appearance, the perovskite solar cell has reached its certified highest efficiency at 25.2% [2]. High absorption coefficient, long diffusion length, low cost, and many material possibilities are the several factors behind perovskite solar cell being extensively investigated and gaining its performance boost [3–5]. Another effort to achieve high-performance perovskite solar cells is by utilizing an organic transport layer spiro-OMETAD. Those transport layers can easily increase the efficiency of perovskite solar cells by around 15% [6]. Despite the achievement of high-performance devices, material instability is still a major concern in perovskite-based solar cells. Water, including that from humidity, can decompose the material of perovskite and degrade solar cell performance rapidly [7]. Furthermore, the organic transport layer also degrades rapidly in an open environment, thereby lessening the age of perovskite solar cells [8]. This drawback makes it rather difficult for perovskite solar cells to enter commercialization.

Several groups of researchers have suggested an engineering modification in the transport layer that can overcome the instability problem, such as the application of a metal oxide transport layer, porous buffer layer, porous transport layer, and nanocrystal transport layer [9–13]. Additionally, the utilization of inorganic materials replaces the usage of expensive complex organic compounds in the transport

layer. Alternatively, other groups proposed an improvement in the perovskite material by partially replacing the I^- ion in perovskite $CH_3NH_3PbI_3$, it came to be known as mixed halide perovskite. Zhang et al. provided information about the stability of mixed halide perovskite by incorporating the SCN^- ion into the perovskite material (normally written as $CH_3NH_3PbI_{3-x}SCN_x$) [14]. Other groups also tried applying the SCN^- ion in perovskite by changing the usage of PbI_2 powder to $Pb(SCN)_2$ in the perovskite precursor, which resulted in an improvement of device stability [15]. The Cl^- ion can also be applied to make mixed halide perovskite $CH_3NH_3PbI_{3-x}Cl_x$. Greater performance and stability can be achieved by using the discussed perovskite rather than pure halide perovskite [16, 17].

However, additive and complex structures were applied in the reported perovskite solar cells. In this research, we fabricated a simple structure of mixed halide perovskite solar cells using a solution-processed fabrication technique. Our devices have a n-i-p structure (FTO/TiO_2/mixed halide perovskite/CuSCN/carbon/FTO) where mixed halide perovskite $CH_3NH_3PbI_{3-x}Cl_x$ and $CH_3NH_3PbI_{3-x}SCN_x$ were utilized as an active layer and inorganic material was used as transport layers. Use of FTO glass-to-FTO glass device configuration also has shown its potential in producing simple and low-cost PSC. Detailed fabrication methods of the devices were also provided. Further, we investigated the performance and stability of both devices to provide a clear report on the application of mixed halide perovskite.

2. Materials and Methods

2.1. Device Structure. Perovskite solar cell was made by following the structure shown in Figure 1. The structure type was n-i-p, where incoming light was passed through the electron transport layer (ETL), which was TiO_2 in this research, before reaching the perovskite layer. This makes the TiO_2 side become the top of the device. TiO_2 as ETL was used because it shows commendable stability as compared to other ETLs, such as ZnO. Although TiO_2 has a more acidic nature than ZnO, it is more thermally stable when used together with perovskite [18]. On the other hand, a wide bandgap (Eg = 3.2 eV) makes TiO_2 transparent, and thus, more light can directly pass through the perovskite layer. For the perovskite layer, mixed halide perovskite $CH_3NH_3PbI_{3-x}Cl_x$ and $CH_3NH_3PbI_{3-x}SCN_x$ were used. The hole transport layer (HTL) in this device was CuSCN. The advantage of using CuSCN was its wide bandgap (Eg = 3.6 eV) and high hole mobility (0.01-0.1 $cm^2V^{-1}s^{-1}$) [19]. Additionally, CuSCN could improve PSC stability [20]. Carbon powder was used to fill the gap or buffer layer between CuSCN and the FTO glass back-contact. In addition, carbon can be used as an electrode and an alternative electrode to Au or Ag [21]. In this device, the carbon powder combined with FTO glass back-contact acted as an electrode [22].

In perovskite solar cells, it is essential to take into account the energy band diagram of each layer. Mismatched energy level from one of the layers hold the potential to block the movement of the electron or hole generated from the perovskite layer. Figure 2 shows an energy level diagram

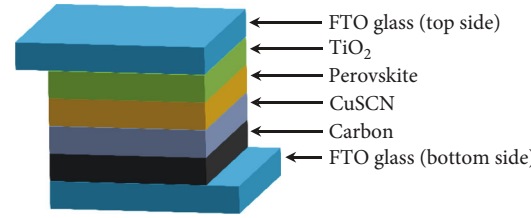

Figure 1: Structure of fabricated devices.

of fabricated devices collected from various research. $CH_3NH_3PbI_{3-x}Cl_x$ has a bandgap of 1.55 eV with an energy level of -3.75 eV for the conduction band and -5.43 eV for the valence band [23]. $CH_3NH_3PbI_{3-x}SCN_x$ has a bandgap of 1.5 eV with a conduction band of -3.93 eV and a valence band of -5.43 eV, similar to pure perovskite $CH_3NH_3PbI_3$ [15]. Wang et al. have provided energy level information for TiO_2 and carbon [24]. TiO_2 has an energy level of -4.1 eV for the conduction band and -7.3 eV for the valence band. Moreover, carbon has an energy level of -5 eV. The energy level for CuSCN was provided as -1.8 eV for the conduction band and -5.4 eV for the valence band [25]. As metal contact, FTO has an energy level of -4.4 eV [7].

2.2. Device Fabrication. In this research, device fabrication was carried out in ambient air. Prior to the deposition using spin coating, a precursor of TiO_2, perovskite, and CuSCN was prepared. The TiO_2 precursor was synthesized by mixing 0.2 M titanium(IV) isopropoxide (TTIP) (97%, Sigma-Aldrich) and 0.1 M hydrochloric acid (HCl) (37%, Merck) into 5 ml of ethanol then stirred for 15 minutes at room temperature. CH_3NH_3I perovskite precursor was synthesized by mixing 8.66 ml of CH_3NH_2 (40 wt. % in H_2O, Sigma-Aldrich) and 13.2 ml of HI (57 wt. % in H_2O, Sigma-Aldrich). The mixed solution was then evaporated with a rotary evaporator for 2 hours until a white dry crystal of CH_3NH_3I formed. Perovskite precursor for both Cl^- and SCN^- mixed halide was synthesized by mixing $PbCl_2$ or $Pb(SCN)_2$ (Sigma-Aldrich) powder and CH_3NH_3I with a molar ratio of 1 : 3, followed by dissolving it in 1 ml of N,N-dimethylformamide (DMF) (≥99.9%, Sigma-Aldrich). Both perovskite precursors were stirred for 1 hour at a temperature of 80°C. As HTL, the CuSCN precursor was made by dissolving 6 mg CuSCN powder (Sigma-Aldrich) in dipropyl sulfide (DPS) (97%, Sigma-Aldrich) and then mixed for 8 hours at room temperature.

The FTO glass (2 × 2 cm^2) was cleaned by an ultrasonic cleaner using three different solutions: deionized water, ethanol, and acetone. Solutions were used to clean the FTO glass for 5 minutes each. Then, the FTO glass was allowed to dry before the deposition using spin coating. The first layer to be deposited was TiO_2 by dropping the TiO_2 precursor on top of the clean FTO glass. The spin coater was spun for 30 seconds, followed by an annealing process using a hotplate with a temperature of 425°C for 30 minutes and left to cool to room temperature. The next deposition was a perovskite layer on top of the FTO/TiO_2 substrate. The perovskite precursor was heated at a temperature of 60°C before the deposition in order to lower the viscosity of the

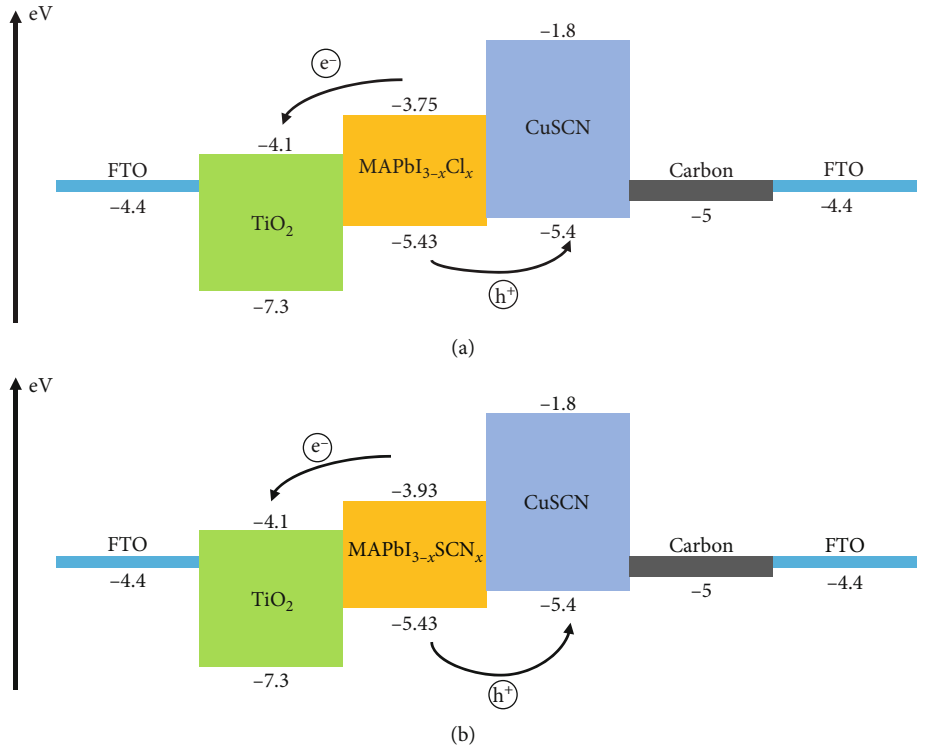

Figure 2: Energy level diagram of perovskite solar cell using (a) $CH_3NH_3PbI_{3-x}Cl_x$ and (b) $CH_3NH_3PbI_{3-x}SCN_x$.

precursor such that the solution could spread evenly. The FTO/TiO_2 substrate was placed in the spin coater and the perovskite precursor was dropped on top of it, followed by spin coating for 30 seconds. Then, the sample was dried using a hotplate at a temperature of 130°C for 15 minutes. When the annealing process was conducted, the yellow solution of perovskite became grey, implying that the perovskite layer was formed. The CuSCN precursor was applied to cover the surface of the perovskite layer by spin coating it for 30 seconds. Afterwards, the annealing process was performed to remove the DPS solution and this resulted in the formation of the CuSCN layer. Finally, carbon powder was placed onto the surface of the CuSCN layer as a buffer layer from the main substrate to the FTO glass back-contact. After the two FTO glasses were clipped together, the active area of the perovskite solar cell was $2 \times 1.5\ cm^2$.

The spin coating rate used in this research was varied to obtain an optimized spin coating rate for each layer. Varied spin coating rate can produce different thicknesses of thin film. The general rule is that when the spin coating rate is high, the thickness of film will decrease because the majority of solvent will be flung off the side. Contrarily, a low spin coating rate will form a thick film because the force is not adequate to throw the solvent off the side as much as the force of a high spin coating rate. For TiO_2, we varied spin the coating rate from 1000–4000 rpm,; for the perovskite layer; it was 500–2000 rpm, and for the CuSCN layer, it was 1000–4000 rpm. After optimization, a fixed spin coating rate was obtained from the highest performance out of all the variations. Afterwards, it was applied to fabricate the perovskite solar cells for performance and stability comparison.

2.3. Measurement. The fabricated solar cells were measured for their dark I-V performance using the Semiconductor Parameter Analyser HP 4145B. In order to determine solar cell performance under illumination, the solar cell was placed outside on a sunny day and then the generated current (I_L) was measured using multimeter. The intensity from the sun was measured using a solar power meter, and the generated current measurement of the solar cell was carried out when the sun intensity was averagely 900 W/m^2. By using Equation (1), information from dark I-V will shift below, corresponding to the generated current [26].

$$I = I_0 \left[\exp\left(\frac{qV}{kT}\right) - 1 \right] - I_{L,} \tag{1}$$

$$\mathrm{FF} = \frac{V_{\mathrm{mp}}\, I_{\mathrm{mp}}}{V_{\mathrm{OC}}\, I_{\mathrm{SC}}}, \tag{2}$$

$$\eta = \frac{V_{\mathrm{OC}}\, I_{\mathrm{SC}}\, \mathrm{FF}}{P_{\mathrm{in}}} \times 100\%. \tag{3}$$

The shifted dark I-V will become a typical I-V curve for solar cells, and therefore, photovoltaic parameters such as open-circuit voltage (V_{OC}), short-circuit current (I_{SC}), maximum power voltage (V_{mp}), and maximum power current (I_{mp}) will be visible. Moreover, fill factor (FF) and efficiency (η) can be calculated by using Equations (2) and (3).

Series resistance (R_{SH}) and shear resistance (R_S) were also provided using the calculation. Before calculating parasitic

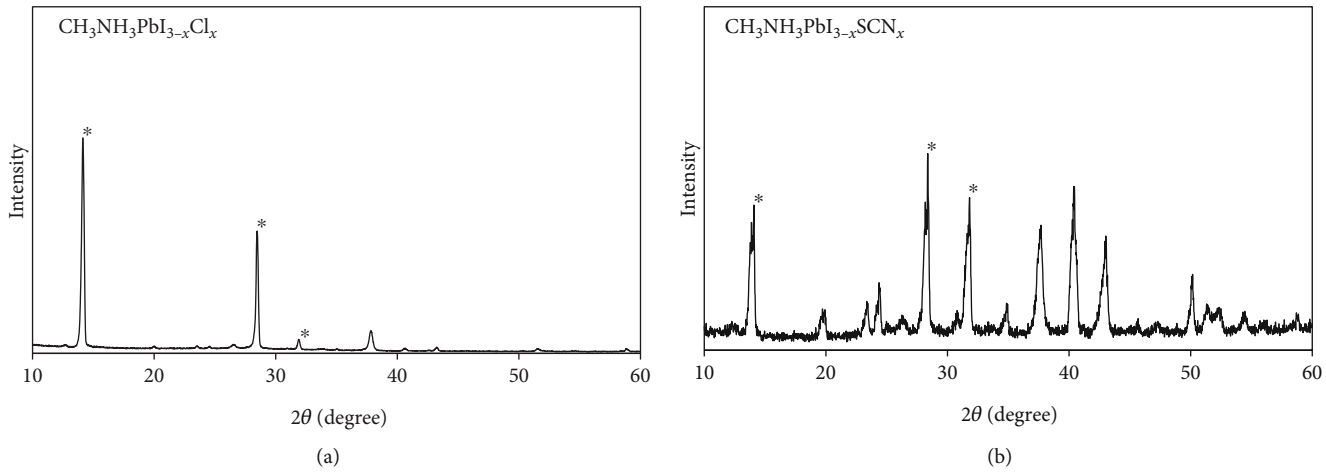

Figure 3: XRD spectra of (a) $CH_3NH_3PbI_{3-x}Cl_x$ and (b) $CH_3NH_3PbI_{3-x}SCN_x$.

resistances, it is essential to calculate normalised V_{OC} (v_{oc}) and normalised FF (FF_0) using the following equation:

$$v_{oc} = \frac{V_{OC}}{(nkT/q)}, \tag{4}$$

$$FF_0 = \frac{v_{oc} - \ln(v_{oc} + 0.72)}{v_{oc} + 1}. \tag{5}$$

Since the fill factor is related to parasitic resistance, normalised R_S (r_s) and normalised R_{SH} (r_{sh}) can be written as Equations (6) and (7), respectively.

$$r_s = \frac{FF_0 - FF}{FF_0}, \tag{6}$$

$$r_{sh} = \frac{FF_0{}^2(v_{oc} + 0.7)}{v_{oc}(FF_0 - FF)}, \tag{7}$$

If the characteristic resistance (R_{CH}) of solar cell is defined in

$$R_{CH} = \frac{V_{OC}}{I_{SC}}, \tag{8}$$

series resistance and shear resistance are given as follows:

$$R_S = r_s R_{CH,} \tag{9}$$

$$R_{SH} = r_{sh} R_{CH.} \tag{10}$$

By substituting Equation (6) into Equation (9), series resistance expression would be given as follows:

$$R_S = \frac{FF_0 - FF}{FF_0} R_{CH.} \tag{11}$$

Similarly, for shunt resistance, by the substitution of Equation (7) into Equation (10), the following can be obtained:

$$R_{SH} = \frac{FF_0{}^2(v_{oc} + 0.7)}{v_{oc}(FF_0 - FF)} R_{CH.} \tag{12}$$

3. Results and Discussion

3.1. Film Characterization. In order to examine whether the deposition process was successful using the prepared precursor, characterization was performed to the fabricated film. Figure 3 shows the X-ray diffraction (XRD) pattern of $CH_3NH_3PbI_{3-x}Cl_x$ and $CH_3NH_3PbI_{3-x}SCN_x$ film on top of the FTO glass. Each perovskite has apparent peaks (2θ) located in 14°, 28°, and 32°, which named planes (110), (220), and (310), respectively (marked with a star). The three peaks correspond to the three lattices of perovskite that are also apparent in perovskite $CH_3NH_3PbI_3$. This shows that the application of $PbCl_2$ or $Pb(SCN)_2$ does not change the crystal structure of perovskite. The other peaks appeared to correspond to the application of those materials [27].

Figure 4 shows the result of energy-dispersive X-ray (EDX) analysis for each material. The EDX was used to demonstrate the presence of ETL, perovskite, and HTL material. TiO_2 was successfully formed with the presence of titanium and oxygen elements (Figure 4(a)). EDX analysis also gave a dominant signal of Pb and I elements, implying that perovskite material exists after the deposition (Figures 4(b) and 4(c)). Furthermore, CuSCN material was also confirmed with the presence of Cu, S, C, and N elements in EDX analysis with a high signal of copper and sulphur elements (Figure 4(d)).

3.2. Layer Optimization. In this research, we optimized the spin coating rate of every layer to obtain decent performance levels for both perovskite solar cells and a comparable sample. A summary of the optimized spin coating rate for this configuration can be found in Table 1.

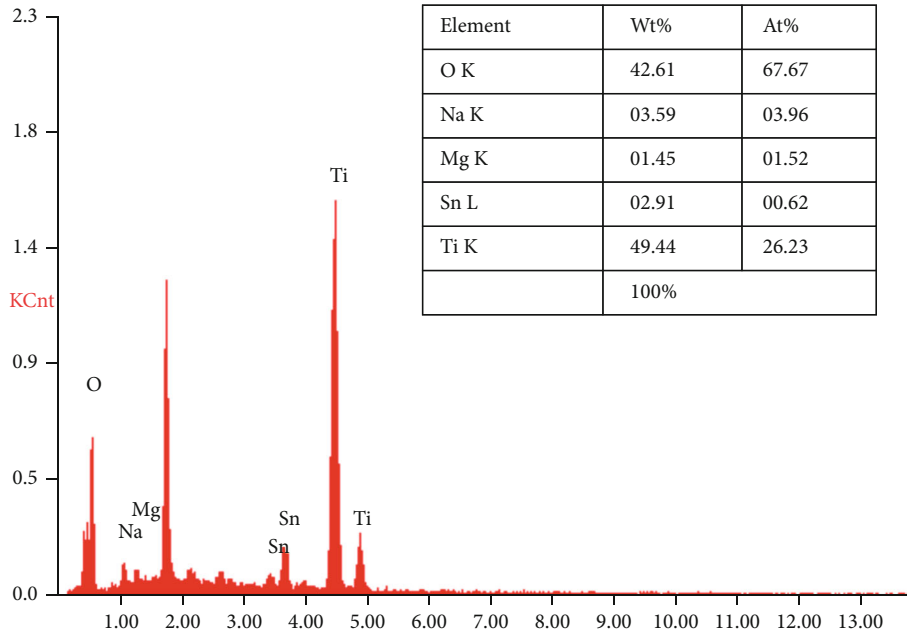

Element	Wt%	At%
O K	42.61	67.67
Na K	03.59	03.96
Mg K	01.45	01.52
Sn L	02.91	00.62
Ti K	49.44	26.23
	100%	

(a)

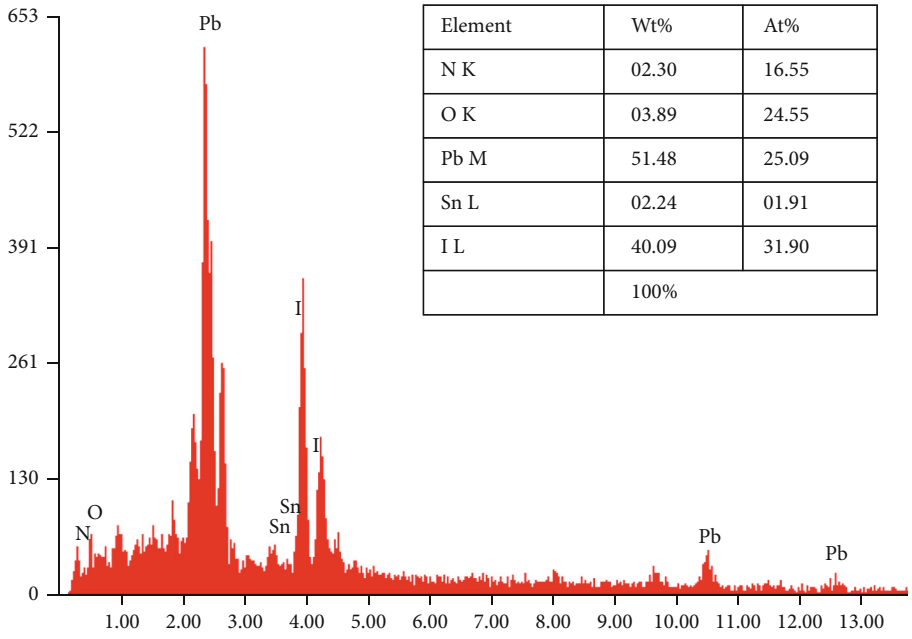

Element	Wt%	At%
N K	02.30	16.55
O K	03.89	24.55
Pb M	51.48	25.09
Sn L	02.24	01.91
I L	40.09	31.90
	100%	

(b)

Figure 4: Continued.

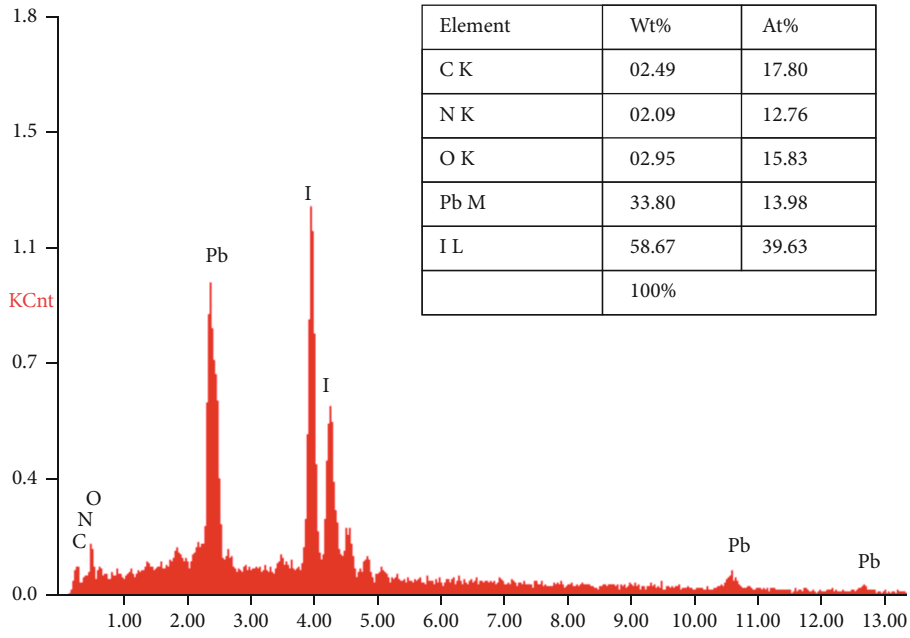

Element	Wt%	At%
C K	02.49	17.80
N K	02.09	12.76
O K	02.95	15.83
Pb M	33.80	13.98
I L	58.67	39.63
	100%	

(c)

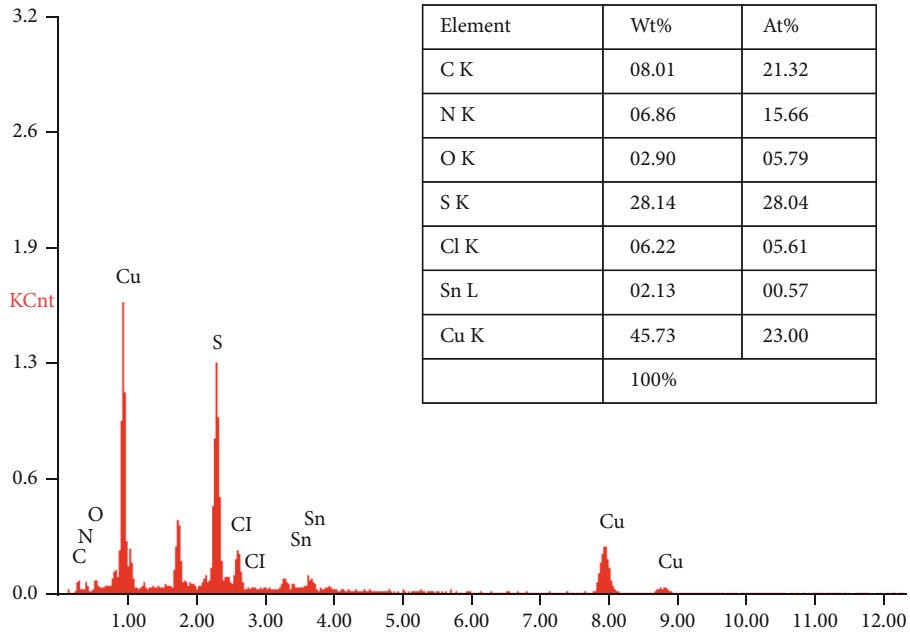

Element	Wt%	At%
C K	08.01	21.32
N K	06.86	15.66
O K	02.90	05.79
S K	28.14	28.04
Cl K	06.22	05.61
Sn L	02.13	00.57
Cu K	45.73	23.00
	100%	

(d)

Figure 4: EDX analysis of (a) TiO_2, (b) $CH_3NH_3PbI_{3-x}Cl_x$, (c) $CH_3NH_3PbI_{3-x}SCN_x$, and (d) CuSCN.

It is worth noting that the spin coating rate can affect the performance of devices in terms of the layer thickness and uniformity formed. In TiO_2, if the layer is too thick from using a low spin coating rate, the electron will travel a greater distance to the metal contact, resulting in increased resistance. Furthermore, the thick TiO_2 layer increases transmittance, which reduces incoming light to the perovskite layer [30]. Those reports are in good agreement with the experiment results where a spin coating rate of 1000 rpm was used in TiO_2, the performance was the lowest among other spin coating rates. On the other hand, a high spin coating rate forms a thinner layer as compared to a slow spin coating rate. If the spin coating rate for TIO_2 is too high, the TiO_2 layer will be too thin, which causes the FTO layer below it to not be covered uniformly. This will create a pinhole and decrease the overall performance of the devices [30]. From the experiment, it was obtained that 3000 rpm is an optimized spin coating rate for TiO_2.

Table 1: Optimized spin coating rate of each layer.

Layer	Spin coating rate (rpm)
TiO_2	3000
$CH_3NH_3PbI_{3-x}Cl_x$ [28]	1000
$CH_3NH_3PbI_{3-x}SCN_x$	1000
CuSCN deposited onto $CH_3NH_3PbI_{3-x}Cl_x$ [29]	2000
CuSCN deposited onto $CH_3NH_3PbI_{3-x}SCN_x$	2000

The thickness of the perovskite layer played a key role in the performance of perovskite solar cells. The spin coating rate optimization was performed for both perovskites with Cl^- and SCN^- to achieve the optimum thickness. It was observed from the experiment that when the lowest spin coating rate (500 rpm) was used, the perovskite layer did not completely transform into grey when the annealing process was finished, which might be caused by an excess of perovskite precursor left in the substrate which in turn might have caused some spot to be too thick; thus, the DMF solvent did not evaporate completely. Wang et al. showed that there was an increase in the performance of the perovskite solar cell when the perovskite thickness was increased. However, if the thickness was too high, it showed a decrease in performance caused by the rough surface of the perovskite [31]. The annealing process can be performed with a higher temperature in order to evaporate the solvent completely. However, higher annealing temperature affected the quality of the perovskite film, thereby decreasing the device's performance [32]. A thin perovskite layer can decrease the performance of perovskite solar cells because there is not enough material to generate electron-hole pairs from the incoming light. In the experiment, the optimum spin coating rate for the perovskite layer in this configuration was found to be 1000 rpm.

Spin coating rate optimization for the CuSCN layer was performed for both layers deposited on top of perovskite with Cl^- as well as SCN^-. Both had an optimum spin coating rate of 2000 rpm. In the case of CuSCN thin film, when the thickness is too thin, the CuSCN surface becomes rough and inhomogeneous [25]. These results have a negative impact on the efficiency of the charge transport.

3.3. Device Performance and Stability. For stability tests, the devices were kept in a dry box with humidity of 25–30% and temperature of 28°C. The devices only placed outside the box when the measurement is conducted. Table 2 shows the performance of two mixed halide perovskite solar cells.

The perovskite solar cells were made by using a fixed spin coating rate from the previous experiment. It shows that the perovskite solar cell with $CH_3NH_3PbI_{3-x}Cl_x$ yields higher efficiency than the SCN^--doped perovskite solar cell. The results are consistent with research conducted by Chen et al. [27]. The external quantum efficiency (EQE) of $CH_3NH_3PbI_{3-x}Cl_x$ is higher at almost all wavelengths, compared to $CH_3NH_3PbI_{3-x}SCN_x$. Higher EQE indicates that more electron-hole pairs will be generated when the incoming light is absorbed by the materials. Furthermore, short-circuit current of the two devices shows compatible results with the aforementioned research. $CH_3NH_3PbI_{3-x}Cl_x$ with short-circuit current of 4.32 mA/cm^2 generates more charge than $CH_3NH_3PbI_{3-x}SCN_x$ with short-circuit current of 2.99 mA/cm^2.

Table 2: Performance of fabricated mixed halide perovskite solar cell.

Perovskite	V_{OC} (V)	J_{SC} (mA/cm^2)	FF	η (%)	R_{sh} (Ω)	R_s (Ω)
$CH_3NH_3PbI_{3-x}Cl_x$	1.16	4.32	0.52	2.92	262.43	49.43
$CH_3NH_3PbI_{3-x}SCN_x$	1.02	2.99	0.59	1.99	407.11	50.91

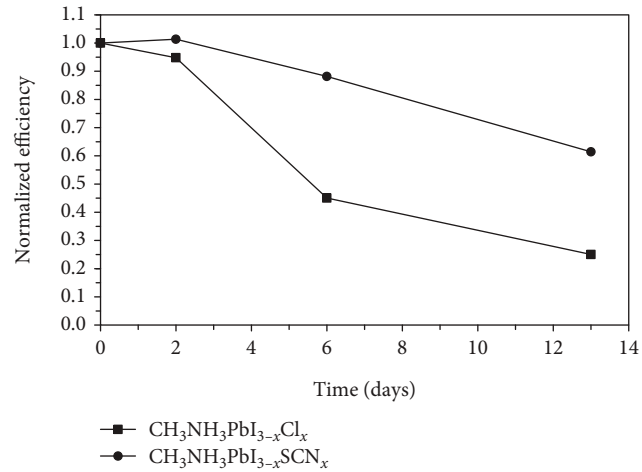

Figure 5: The stability test of perovskite solar cell using $CH_3NH_3PbI_{3-x}Cl_x$ (circle) and $CH_3NH_3PbI_{3-x}SCN_x$ (square) for 13 days.

To analyze performance stability by time, the sample was stored in a dry box with a humidity level of 18%–20% and measured periodically for 13 days. Perovskite solar cells were taken outside the dry box only for measurement. The changes in the efficiency of fabricated devices are shown in Figure 5.

The results show that the solar cell $CH_3NH_3PbI_{3-x}SCN_x$ possessed better stability compared to the Cl^--based perovskite solar cell. On day two, there was a slight increase in the efficiency for solar cells using $CH_3NH_3PbI_{3-x}SCN_x$. This might have been caused by the safe condition where the humidity was lower or drier from ambient. Research by Leguy et al. reveals that humidity in perovskite solar cells can be removed by drying the devices [33]. Contrarily, the solar cell using $CH_3NH_3PbI_{3-x}Cl_x$ shows a decrease in performance by 5% from its initial efficiency. Days 6 and 13 show a performance decrease for both samples. However, on day 13, the SCN^--based perovskite solar cell exhibits greater stability with only 39% degradation in efficiency, compared to solar cell $CH_3NH_3PbI_{3-x}Cl_x$ with 61% degradation. The changes of photovoltaic parameters for 13 days are summarized in Table 3.

Furthermore, the decrease in the fill factor of solar cells using $CH_3NH_3PbI_{3-x}Cl_x$ is also shown in the I-V curve of

Table 3: Changes in photovoltaic parameters of perovskite solar cell using $CH_3NH_3PbI_{3-x}Cl_x$ and $CH_3NH_3PbI_{3-x}SCN_x$.

Days	$CH_3NH_3PbI_{3-x}Cl_x$				$CH_3NH_3PbI_{3-x}SCN_x$			
	V_{OC} (V)	J_{SC} (mA/cm^2)	FF	η (%)	V_{OC} (V)	J_{SC} (mA/cm^2)	FF	η (%)
0	1.16	4.32	0.52	2.92	1.02	2.99	0.59	1.99
2	1.22	4.09	0.50	2.77	1.02	3.12	0.57	2.02
6	1.02	2.44	0.48	1.31	0.98	2.71	0.59	1.75
13	0.94	1.80	0.39	0.73	0.92	2.08	0.57	1.22

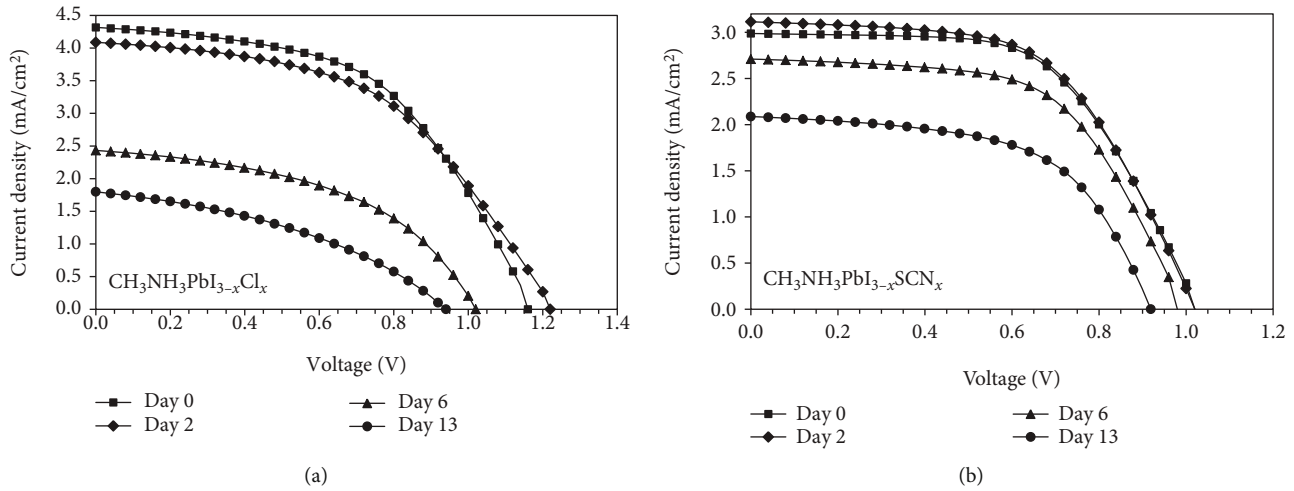

Figure 6: Current-voltage (I-V) characteristics of perovskite solar cell using (a) $CH_3NH_3PbI_{3-x}Cl_x$ and (b) $CH_3NH_3PbI_{3-x}SCN_x$ showing changes of I-V curve shape and decreasing short-circuit current and open-circuit voltage for 13 days.

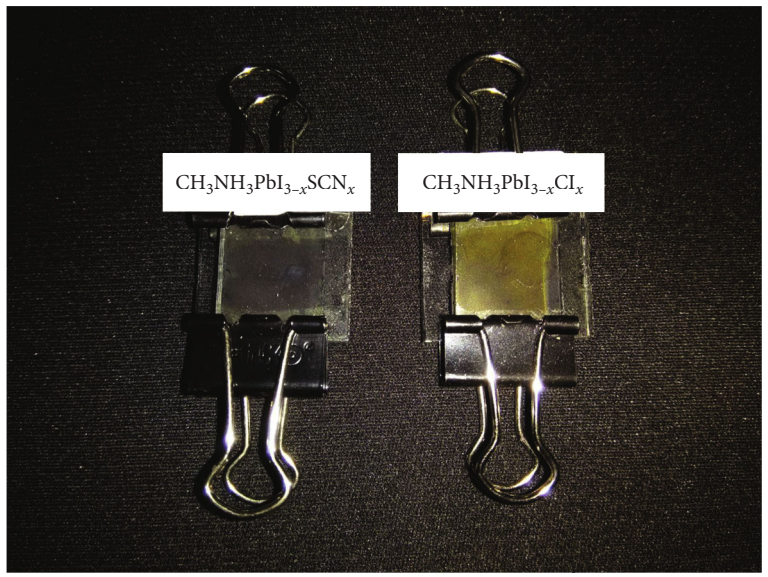

Figure 7: Decomposition of perovskite layer seen on day 13.

the stability test (Figure 6(a)). Decrease in the fill factor makes the I-V curve's shape more linear. On the other hand, SCN-based perovskite solar cells did not show a significant decrease in the fill factor, which leads to a consistent I-V curve shape (Figure 6(b)).

Perovskite solar cell decomposition can be seen visually through the changes of colour in the perovskite layer from dark grey to yellow. This degradation is shown in Figure 7. On day 13 days, it is visible that the colour of Cl-based perovskite solar cell turned back into yellow. This finding is significantly in agreement with the stability test data where the performance degradation of $CH_3NH_3PbI_{3-x}Cl_x$ is much faster and greater compared to $CH_3NH_3PbI_{3-x}SCN_x$. Perovskite $CH_3NH_3PbI_{3-x}SCN_x$ has good stability

because SCN^- has an ionic bond with Pb^{2+} and a hydrogen bond with $CH_3NH_2^+$ [15].

Compared to pure halide perovskite ($CH_3NH_3PbI_3$), Cl-based perovskite also has greater stability [16]. Moreover, its stability was provided by its better crystallinity and morphology. The results show that chemically stable perovskite $CH_3NH_3PbI_{3-x}SCN_x$ exhibits better stability than perovskite $CH_3NH_3PbI_{3-x}Cl_x$ does.

4. Conclusions

In conclusion, the performance and stability of solar cells using mixed halide perovskite $CH_3NH_3PbI_{3-x}Cl_x$ and $CH_3NH_3PbI_{3-x}SCN_x$ were demonstrated. It was found that solar cells using $CH_3NH_3PbI_{3-x}Cl_x$ have a better performance rate as compared to SCN^--based perovskite solar cells with V_{OC} of 1.16 V, I_{SC} of 4.32 mA/cm^2, FF of 0.52, and an efficiency of 2.92%. The stability test shows that perovskite solar cells using $CH_3NH_3PbI_{3-x}SCN_x$ yield better stability with only 39% degradation from its initial efficiency in comparison with another mixed halide perovskite solar cell.

Data Availability

All data used to support the findings of this study are included within the article.

Conflicts of Interest

The authors declare that they have no conflict of interest.

Acknowledgments

This work has been supported by the Ministry of Research, Technology and Higher Education of the Republic of Indonesia under Grant No. NKB-354/UN2.RST/HKP.05.00/2020 and Directorate of Innovation and Science Techno Park Universitas Indonesia under Grant of Design and Prototyping Development P5 2020.

References

[1] A. Kojima, K. Teshima, Y. Shirai, and T. Miyasaka, "Organometal halide perovskites as visible- light sensitizers for photovoltaic cells," *Journal of the American Chemical Society*, vol. 131, no. 17, pp. 6050-6051, 2009.

[2] M. A. Green, E. D. Dunlop, J. Hohl-Ebinger, M. Yoshita, N. Kopidakis, and A. W. Y. Ho-Baillie, "Solar cell efficiency tables (version 55)," *Progress in Photovoltaics: Research and Applications*, vol. 28, no. 1, pp. 3–15, 2020.

[3] Q. Lin, A. Armin, R. C. R. Nagiri, P. L. Burn, and P. Meredith, "Electro-optics of perovskite solar cells," *Nature Photonics*, vol. 9, no. 2, pp. 106–112, 2015.

[4] C. Wehrenfennig, M. Liu, H. J. Snaith, M. B. Johnston, and L. M. Herz, "Charge-carrier dynamics in vapour-deposited films of the organolead halide perovskite $CH_3NH_3PbI_{3-x}Cl_x$," *Energy & Environmental Science*, vol. 7, no. 7, pp. 2269–2275, 2014.

[5] H. J. Snaith, "Perovskites: the emergence of a new era for low-cost, high-efficiency solar cells," *Journal of Physical Chemistry Letters*, vol. 4, no. 21, pp. 3623–3630, 2013.

[6] J. Zheng, M. Zhang, C. F. J. Lau et al., "Spin-coating free fabrication for highly efficient perovskite solar cells," *Solar Energy Materials and Solar Cells*, vol. 168, pp. 165–171, 2017.

[7] I. Mesquita, L. Andrade, and A. Mendes, "Perovskite solar cells: materials, configurations and stability," *Renewable and Sustainable Energy Reviews*, vol. 82, pp. 2471–2489, 2018.

[8] S. N. Habisreutinger, T. Leijtens, G. E. Eperon, S. D. Stranks, R. J. Nicholas, and H. J. Snaith, "Carbon nanotube/polymer composites as a highly stable hole collection layer in perovskite solar cells," *Nano Letters*, vol. 14, no. 10, pp. 5561–5568, 2014.

[9] J. You, L. Meng, T. B. Song et al., "Improved air stability of perovskite solar cells via solution-processed metal oxide transport layers," *Nature Nanotechnology*, vol. 11, no. 1, pp. 75–81, 2016.

[10] E. H. Anaraki, A. Kermanpur, L. Steier et al., "Highly efficient and stable planar perovskite solar cells by solution-processed tin oxide," *Energy & Environmental Science*, vol. 9, no. 10, pp. 3128–3134, 2016.

[11] S. Guarnera, A. Abate, W. Zhang et al., "Improving the long-term stability of perovskite solar cells with a porous Al_2O_3 buffer layer," *Journal of Physical Chemistry Letters*, vol. 6, no. 3, pp. 432–437, 2015.

[12] Z. Zhu, Y. Bai, X. Liu, C.-C. Chueh, S. Yang, and A. K.-Y. Jen, "Enhanced efficiency and stability of inverted perovskite solar cells using highly crystalline SnO_2 nanocrystals as the robust electron-transporting layer," *Advanced Materials*, vol. 28, no. 30, pp. 6478–6484, 2016.

[13] F. T. F. O'Mahony, Y. H. Lee, C. Jellett et al., "Improved environmental stability of organic lead trihalide perovskite-based photoactive-layers in the presence of mesoporous TiO_2," *Journal of Materials Chemistry A*, vol. 3, no. 14, pp. 7219–7223, 2015.

[14] Z. Zhang, Y. Zhou, Y. Cai et al., "Efficient and stable $CH_3NH_3PbI_{3-x}(SCN)_x$ planar perovskite solar cells fabricated in ambient air with low-temperature process," *Journal of Power Sources*, vol. 377, pp. 52–58, 2018.

[15] Q. Tai, P. You, H. Sang et al., "Efficient and stable perovskite solar cells prepared in ambient air irrespective of the humidity," *Nature Communications*, vol. 7, no. 1, article 11105, 2016.

[16] N. Tripathi, M. Yanagida, Y. Shirai, T. Masuda, L. Han, and K. Miyano, "Hysteresis-free and highly stable perovskite solar cells produced via a chlorine-mediated interdiffusion method," *Journal of Materials Chemistry A*, vol. 3, no. 22, pp. 12081–12088, 2015.

[17] Y. Wang, T. Mahmoudi, W. Y. Rho et al., "Ambient-air-solution-processed efficient and highly stable perovskite solar cells based on $CH_3NH_3PbI_{3-x}Cl_x$-NiO composite with Al_2O_3/NiO interfacial engineering," *Nano Energy*, vol. 40, pp. 408–417, 2017.

[18] J. Yang, B. D. Siempelkamp, E. Mosconi, F. De Angelis, and T. L. Kelly, "Origin of the thermal instability in $CH_3NH_3PbI_3$ Thin films deposited on ZnO," *Chemistry of Materials*, vol. 27, no. 12, pp. 4229–4236, 2015.

[19] P. Pattanasattayavong, G. O. N. Ndjawa, K. Zhao et al., "Electric field-induced hole transport in copper(i) thiocyanate (CuSCN) thin-films processed from solution at room temperature," *Chemical Communications*, vol. 49, no. 39, pp. 4154–4156, 2013.

[20] N. Arora, M. I. Dar, A. Hinderhofer et al., "Perovskite solar cells with CuSCN hole extraction layers yield stabilized efficiencies greater than 20%," *Science*, vol. 358, no. 6364, pp. 768–771, 2017.

[21] R. He, X. Huang, M. Chee, F. Hao, and P. Dong, "Carbon-based perovskite solar cells: from single-junction to modules," *Carbon Energy*, vol. 1, no. 1, pp. 109–123, 2019.

[22] Rembianov, L. Kevin, J. Sulistianto, and N. R. Poespawati, "Activated carbon as the counter electrode on perovskite solar cells," in *2019 11th International Conference on Information Technology and Electrical Engineering (ICITEE)*, vol. 7, pp. 1–4, Pattaya, Thailand, October 2019.

[23] S. A. Bretschneider, J. Weickert, J. A. Dorman, and L. Schmidt-Mende, "Research update: physical and electrical characteristics of lead halide perovskites for solar cell applications," *APL Materials*, vol. 2, no. 4, article 040701, 2014.

[24] H. Wang, X. Hu, and H. Chen, "The effect of carbon black in carbon counter electrode for $CH_3NH_3PbI_3/TiO_2$ heterojunction solar cells," *RSC Advances*, vol. 5, no. 38, pp. 30192–30196, 2015.

[25] J. W. Jung, C. C. Chueh, and A. K. Y. Jen, "High-performance semitransparent perovskite solar cells with 10% power conversion efficiency and 25% average visible transmittance based on transparent CuSCN as the hole-transporting material," *Advanced Energy Materials*, vol. 5, no. 17, article 1500486, 2015.

[26] S. R. Wenham, M. A. Green, M. E. Watt, and R. Corkish, *Applied Photovoltaics*, Routledge, London, 2nd edition, 2007.

[27] S. Chen, B. Chen, X. Gao et al., "Neutral-colored semitransparent solar cells based on pseudohalide (SCN^-)-doped perovskite," *Sustainable Energy & Fuels*, vol. 1, no. 5, pp. 1034–1040, 2017.

[28] M. Hariadi, I. Dzikri, R. W. Purnamaningsih, and N. R. Poespawati, "Fabrication of low cost perovskite solar cell under ambient conditions using only spin coating deposition method," *E3S Web of Conferences*, vol. 67, article 01022, 2018.

[29] J. Sulistianto, R. W. Purnamaningsih, and N. R. Poespawati, "Optimization of rotation speed for CuSCN hole transport layer in perovskite solar cell using spin coating," *Journal of Physics Conference Series*, vol. 1195, article 012025, 2019.

[30] H. Liu, H. Bala, B. Zhang et al., "Thickness-dependent photovoltaic performance of TiO_2 blocking layer for perovskite solar cells," *Journal of Alloys and Compounds*, vol. 736, pp. 87–92, 2018.

[31] K. Wang, C. Liu, P. du et al., "Efficiencies of perovskite hybrid solar cells influenced by film thickness and morphology of $CH_3NH_3PbI_3-_xCl_x$ layer," *Organic Electronics*, vol. 21, pp. 19–26, 2015.

[32] L. C. Chen, C. C. Chen, J. C. Chen, and C. G. Wu, "Annealing effects on high-performance $CH_3NH_3PbI_3$ perovskite solar cells prepared by solution-process," *Solar Energy*, vol. 122, pp. 1047–1051, 2015.

[33] A. M. A. Leguy, Y. Hu, M. Campoy-Quiles et al., "Reversible hydration of $CH_3NH_3PbI_3$ in films, single crystals, and solar cells," *Chemistry of Materials*, vol. 27, no. 9, pp. 3397–3407, 2015.